

Janus monolayers Fe_2SSeX_2(X = Ga, In, and Tl): Robust nontrivial topology with high Chern number

Kang Jia(贾康), Xiao-Jing Dong(董晓晶), Pei-Ji Wang(王培吉), and Chang-Wen Zhang(张昌文)
Citation: Chin. Phys. B, 2024, 33 (**12**): 127103. DOI: 10.1088/1674-1056/ad7c2a
Journal homepage: http://cpb.iphy.ac.cn; http://iopscience.iop.org/cpb

What follows is a list of articles you may be interested in

Half-metallic ferromagnetic Weyl fermions related to dynamic correlations in the zinc-blende compound VAs

Xianyong Ding(丁献勇), Haoran Wei(魏皓然), Ruixiang Zhu(朱瑞翔), Xiaoliang Xiao(肖晓亮), Xiaozhi Wu(吴小志), and Rui Wang(王锐)
Chin. Phys. B, 2024, 33 (**9**): 097103. DOI: 10.1088/1674-1056/ad5f86

Discovery of controllable high Chern number quantum anomalous Hall state in tetragonal lattice FeSIn

Xiao-Lang Ren(任小浪) and Chang-Wen Zhang(张昌文)
Chin. Phys. B, 2024, 33 (**6**): 067102. DOI: 10.1088/1674-1056/ad2bf1

Coexistence of Dirac and Weyl points in non-centrosymmetric semimetal $NbIrTe_4$

Qingxin Liu(刘清馨), Yang Fu(付阳), Pengfei Ding(丁鹏飞), Huan Ma(马欢), Pengjie Guo(郭朋杰), Hechang Lei(雷和畅), and Shancai Wang(王善才)
Chin. Phys. B, 2024, 33 (**4**): 047104. DOI: 10.1088/1674-1056/ad2a79

Exploration of growth conditions of TaAs Weyl semimetal thin film using pulsed laser deposition

Shien Li(李世恩), Zefeng Lin(林泽丰), Wei Hu(胡卫), Dayu Yan(闫大禹), Fucong Chen(陈赋聪), Xinbo Bai(柏欣博), Beiyi Zhu(朱北沂), Jie Yuan(袁洁), Youguo Shi(石友国), Kui Jin(金魁), Hongming Weng(翁红明), and Haizhong Guo(郭海中)
Chin. Phys. B, 2023, 32 (**4**): 047103. DOI: 10.1088/1674-1056/acb913

Maximum entropy mobility spectrum analysis for the type-I Weyl semimetal TaAs

Wen-Chong Li(李文充), Ling-Xiao Zhao(赵凌霄), Hai-Jun Zhao(赵海军),Gen-Fu Chen(陈根富), and Zhi-Xiang Shi(施智祥)
Chin. Phys. B, 2022, 31 (**5**): 057103. DOI: 10.1088/1674-1056/ac2b24

Janus monolayers Fe_2SSeX_2 (X = Ga, In, and Tl): Robust nontrivial topology with high Chern number

Kang Jia(贾康)[1,2], Xiao-Jing Dong(董晓晶)[1], Pei-Ji Wang(王培吉)[1], and Chang-Wen Zhang(张昌文)[1,2,†]

[1] *School of Physics and Technology, Institute of Spintronics, University of Jinan, Jinan* 250022, *China*
[2] *School of Physics and Physical Engineering, Qufu Normal University, Qufu* 273165, *China*

(Received 29 May 2024; revised manuscript received 15 September 2024; accepted manuscript online 18 September 2024)

High-performance quantum anomalous Hall (QAH) systems are crucial materials for exploring emerging quantum physics and magnetic topological phenomena. Inspired by layered FeSe materials with excellent superconducting properties, the Janus monolayers Fe_2SSeX_2 (X = Ga, In and Tl) are built by the decoration of Ga, In and Tl atoms in monolayer Fe_2SSe. In first-principles calculations, Fe_2SSeX_2 have stable structures and prefer ferromagnetic (FM) ordering, and can be considered as Weyl semimetals without spin–orbit coupling. For out-of-plane (OOP) magnetic anisotropy, large nontrivial gaps are opened and the Fe_2SSeX_2 are predicted to be large-gap QAH insulators with a high Chern number $C = 2$, proved by two chiral edge states and Berry curvature. When the magnetization is flipped, the two chiral edge states can be simultaneously changed and $C = -2$ can be obtained, revealing the fascinating behavior of chiral spin–edge state locking. It is found that the QAH properties of Fe_2SSeX_2 are robust against strain. In particular, nontrivial topological quantum states can spontaneously appear for Fe_2SSeGa_2 and Fe_2SSeIn_2 because the orientations of the easy magnetic axis are adjusted from in-plane to OOP by the biaxial strain. Our studies provide excellent candidate systems to realize QAH properties with a high Chern number, and suggest more experimental explorations combining superconductivity and topology.

Keywords: Weyl semimetal, high Chern number, chiral spin–edge state locking, robust

PACS: 71.15.–m, 75.30.Gw, 85.75.–d **DOI:** 10.1088/1674-1056/ad7c2a

1. Introduction

In materials science and condensed matter physics, the exploration of high-performance two-dimensional (2D) quantum anomalous Hall (QAH) materials is currently an attractive topic.[1–3] Because it exhibits quantized Hall conductance in the absence of magnetic fields,[4] a QAH system with topologically nontrivial electronic structure belongs to a novel quantum state distinct from traditional insulators. In particular, no symmetry protections exist in a QAH system. QAH insulators have been realized in many magnetically doped systems such as transition metal dichalcogenide heterobilayers,[5] $MnBi_2Te_4$[6] and twisted bilayer graphene.[7] The magnetic topological quantum states offer a broad platform for investigating multi-functional and low-power electronic devices. However, the ultra low critical temperature severely restricts practical applications and experimental exploration, so it is vital to seek high-temperature QAH materials. Weyl semimetals possess crossing linear energy bands at the Fermi level and have many excellent traits, such as surface states, large negative magnetoresistance and the anomalous Hall effect.[8,9] Since three-dimensional (3D) Weyl semimetals have been widely investigated,[8,9] some researchers have proposed Weyl semimetals based on 2D materials,[10–12] where the Weyl points are formed by the same spin channel and time-reversal symmetry is broken. The $PtCl_3$ monolayer was considered to be a 2D Weyl semimetal by You *et al.*[10] Because Weyl fermions and a half-metallic ferromagnetic (FM) state are combined in Weyl semimetals, they have widespread applications in spintronics and topological nanodevices. Moreover, compared with 3D systems, 2D materials have lower symmetries, so the occurrence of Weyl points is very difficult. Compared with previous related investigations in spintronics and valleytronics,[13–20] the exploration of novel 2D systems with intriguing Weyl semimetal properties is significant.

Very recently, on account of some fascinating superconducting features, layered Fe-based materials have aroused wide interest in both theory and experiment.[21–26] One group of candidates is layered FeSe compounds with weak van der Waals interaction. Metal atoms such as Li and Tl were intercalated in bulk FeSe,[22,23] which shows superconducting properties. The superconducting critical temperatures of the FeSe thin films were enhanced. For instance, when FeSe films were fabricated on one doped $SrTiO_3$ substrate,[26] superconducting features were discovered above 100 K. Nevertheless, up to now, the topological properties of FeSe films have seldom been researched. Accompanied by advanced experimental technologies,[21,25,26] FeSe monolayers represent a new candidate material for researching novel topological electronic structures such as Weyl semimetals, QAH systems[27,28] and quantum spin Hall effects.[29–31] Apart from the temperature challenge, the nontrivial topology with a high Chern number is another important factor,[32–36] and it is intriguing and challenging to seek materials with a high Chern number.

†Corresponding author. E-mail: ss_zhangchw@ujn.edu.cn

© 2024 Chinese Physical Society and IOP Publishing Ltd

In this work, by using first-principles calculations, the Janus monolayers Fe_2SSeX_2 (X = Ga, In and Tl) are found to be potential large-gap QAH insulators. The stabilities are verified by *ab initio* molecular dynamics (AIMD) simulations, phonon spectra and formation energy. We systematically investigate the electronic, magnetic and topological properties. The Fe_2SSeX_2 monolayers have Weyl semimetal features without spin–orbit coupling (SOC). Remarkably, with out-of-plane (OOP) magnetic anisotropy, a high Chern number $C = 2$ can be observed in the FM ground state. When the magnetization is reversed, the Dirac cones are provided by spin-up channels and $C = -2$ is calculated, showing the attractive behavior of chiral spin–edge state locking. Very significantly, the easy magnetic axis direction can be adjusted by biaxial strain. It is hoped that our theoretical work can offer broad platforms for multifunctional quantum devices.

2. Computational details

Based on density functional theory, first-principles calculations were performed using the projected augmented wave method,[37] as implemented in the Vienna *ab initio* simulation package.[38,39] The electronic exchange–correlation interactions were handled by the generalized gradient approximation (GGA) of Perdew–Burke–Ernzerhof.[40] The kinetic cutoff energy was set to 500 eV. A vacuum layer of 23 Å was employed to avoid interactions between the periodic structures. The convergence criteria of atomic force and total energy were 0.01 eV·Å^{-1} and 10^{-6} eV, respectively. For the primitive unit cell and $2\times2\times1$ supercell, the first Brillouin zone was sampled with $17\times17\times1$ and $11\times11\times1$ Γ-centered k-grids, respectively. The GGA+U method[41] was used to correct the Coulomb repulsion interactions of Fe 3d orbitals. According to previous reports, $U = 3$ eV was chosen.[42] The phonon spectra were calculated in the PHONOPY code[43,44] using a $4\times4\times1$ supercell. AIMD simulations with a $4\times4\times1$ supercell at 300 K were performed. The maximally localized Wannier functions were constructed through the WANNIER90 package[45,46] and the Berry curvature and edge state were calculated using the WannierTools package.[47]

3. Results and discussion

It is well known that monolayer FeSe has a tetragonal lattice with the space group $P4/nmm$ (No. 129). Each unit cell is composed of two Se and two co-planar Fe atoms. Significantly, Janus monolayer MoSSe has been experimentally constructed from monolayer MoS_2.[48] One idea appears to be to build the Janus monolayer Fe_2SSe by substituting one of two Se layers with S atoms. Analogous to LiFeSe monolayers,[49] Fe_2SSeX_2 monolayers are constructed by the decoration of Fe_2SSe with Ga, In and Tl. As illustrated in Figs. 1(a) and 1(b), these structures contain X–S–Fe–Se–X quintuple layers and have the $P4mm$ space group (No. 99). The primary space-group symmetry operations of monolayer LiFeSe involve M_x and M_y mirrors, C_4 rotation, space inversion P and one glide mirror $G_z = \{M_z|0.5,0.5,0\}$.[49] Specifically, for Fe_2SSeX_2, the space inversion P and glide mirror G_z are dismissed. The optimized lattice constants (a) of Fe_2SSeGa_2, Fe_2SSeIn_2 and Fe_2SSeTl_2 are 3.83 Å, 3.87 Å and 3.95 Å, respectively (see Table 1), which can be explained by the increasing atomic radius from Ga to Tl. Phonon spectra and AIMD simulations were used to evaluate the dynamical and thermal stabilities, respectively. As shown in Figs. S1(a)–S1(c), for the whole Brillouin zone no imaginary phonon frequency is observed, which suggests the dynamical stability of Fe_2SSeX_2. The intact structures can be obtained after a 6 ps AIMD simulation at 300 K (see Figs. S1(d)–S1(f)), confirming thermal stability at room temperature. The formation energy E_f is calculated by

$$E_f = \left(2E_{Fe} + E_S + E_{Se} + 2E_X - E_{Fe_2SSeX_2}\right)/6. \quad (1)$$

Here $E_{Fe_2SSeX_2}$, E_{Fe}, E_S, E_{Se} and E_X are the energies of Fe_2SSeX_2 and the Fe crystal, S crystal, Se crystal and X crystal, respectively. As listed in Table 1, the acquired formation energies show that these processes are exothermic reactions, demonstrating that experimental syntheses are realizable.

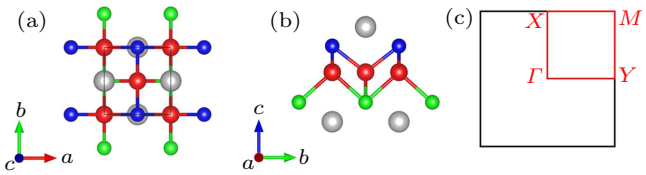


Fig. 1. (a) Top and (b) side views of Fe_2SSeX_2. The red, blue, green and gray balls represent Fe, S, Se and X (X = Ga, In and Tl) elements, respectively. (c) The Brillouin zone.

Table 1. The optimized lattice constants (a), formation energy (E_f), anisotropy constants (K_1 and K_2), magnetocrystalline anisotropy energy (MAE), nearest-neighbor exchange parameter (J), magnetic transition temperature (T), distance of the nearest-neighbor Fe–Fe atoms (d_{Fe-Fe}), the bond angles (α) of Fe–S–Fe and Fe–Se–Fe ($\alpha_{Fe-S-Fe}$ and $\alpha_{Fe-Se-Fe}$), Fermi velocity (υ_f), and band gap (E_g) for Fe_2SSeX_2.

	Fe_2SSeGa_2	Fe_2SSeIn_2	Fe_2SSeTl_2
a (Å)	3.83	3.87	3.95
E_f (eV)	0.68	0.54	0.59
K_1 (μeV)	93.78	39.47	4009.45
K_2 (μeV)	72.81	9.60	715.13
MAE (μeV)	–177	–50	–4731
J (meV)	73.13	59.69	49.06
T (K)	755	616	506
d_{Fe-Fe} (Å)	2.71	2.73	2.79
$\alpha_{Fe-S-Fe}$ (°)	104.1	106.1	108.9
$\alpha_{Fe-Se-Fe}$ (°)	96.5	97.4	100.3
υ_f (10^5 m·s^{-1})	5.1	4.8	3.5
E_g (meV)	174	199	112

The magnetic properties of Fe_2SSeX_2 are now explored. The considered FM and five representative antiferromagnetic (AFM) configurations are displayed in Fig. S2 in the supplemental material. We calculated the total energies of the

different magnetic configurations (see Tables S1–S3). For Fe_2SSeX_2, compared with the energies of five AFM states, it is clearly seen that the total energy of the FM state is lower. Hence, Fe_2SSeX_2 prefer FM exchange coupling. Because the partly filled d orbitals of transition metal elements commonly result in magnetism, Fe_2SSeGa_2 is discussed as one illustrative example to comprehend the magnetic features. Clearly, as observed in Figs. 2(a) and 2(b), the spin-down d orbitals of Fe atoms dominate the energy bands around the Fermi level. Crossed energy bands can be discovered in the Fermi level, leading to the occurrence of Weyl semimetal features in Fe_2SSeX_2.

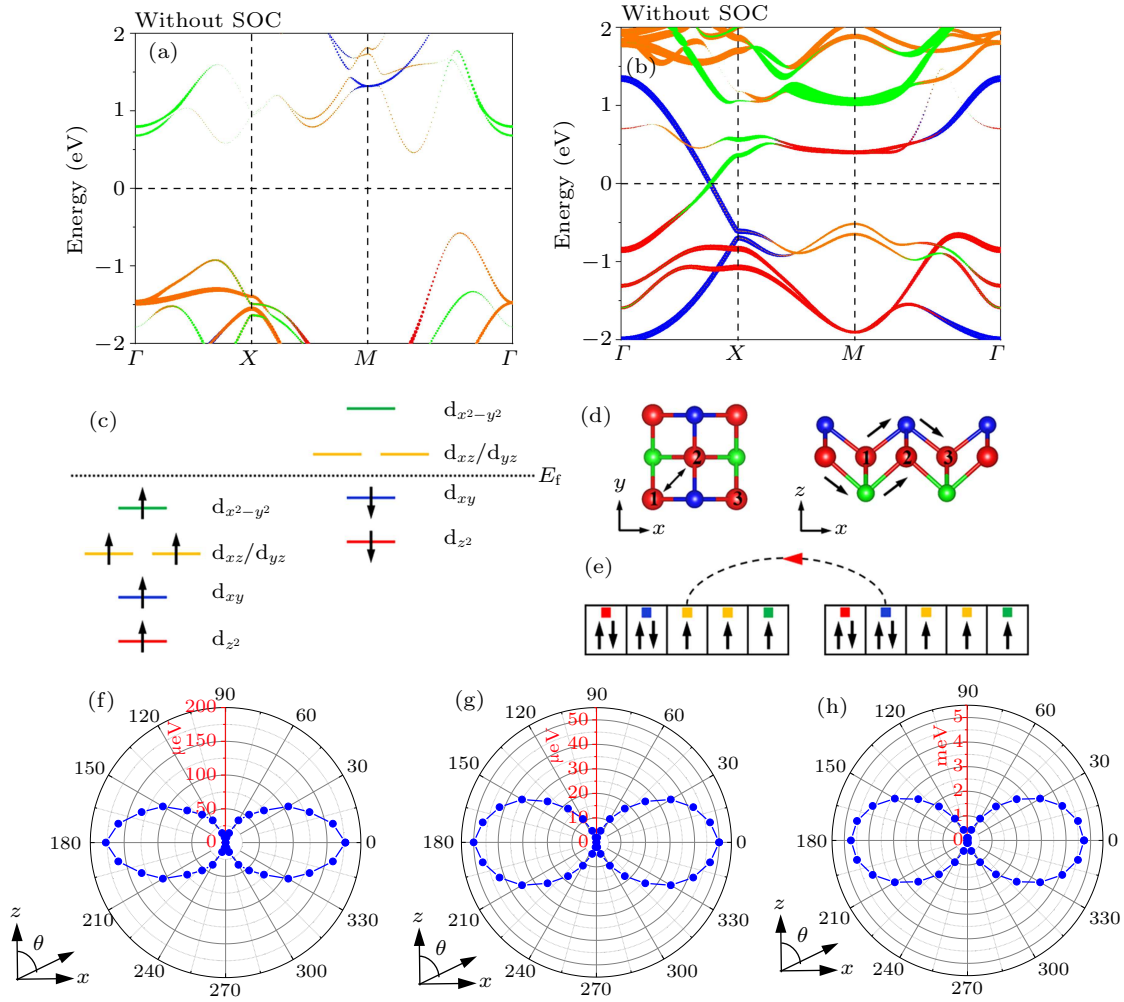


Fig. 2. The d-orbital character energy band structures in (a) spin-up and (b) spin-down states of the Fe_2SSeGa_2 without considering SOC. The red, blue, green and orange dots signify d_{z^2}, d_{xy}, $d_{x^2-y^2}$ and d_{xz}/d_{yz} orbitals of Fe, respectively. (c) Schematic of d orbital occupations for Fe in Fe_2SSeX_2. (d) Schematic of direct-exchange interaction between nearest-neighbor Fe atoms and super-exchange interaction between next-nearest-neighbor Fe atoms. (e) Schematic of ferromagnetic direct-exchange interaction between nearest-neighbor Fe when the Fe 3d orbitals are almost completely occupied. (f)–(h) The energies of the unit cell versus angle (θ) for Fe_2SSeGa_2, Fe_2SSeIn_2 and Fe_2SSeTl_2, respectively. The energy of IP magnetization is set as zero.

The density of states (DOS) is plotted in Fig. S3. The entire overlaps of the Fe d_{xz} and d_{yz} orbitals in the DOS are attributed to the C_{4v} point group in Fe_2SSeX_2. The p_x and p_y orbitals of S and Se possess identical features. According to Fig. S3, both Fe 4s and Ga 4p orbitals contribute one electron, and these electrons are respectively donated to the S 3p and Se 4p orbitals, meaning that the S 3p and Se 4p orbitals are almost completely filled (see Figs. S3(c) and (d)). Moreover, the FM exchange coupling mainly stems from the Fe 3d orbitals due to the completely occupied spin-up Fe 3d orbitals and partly filled spin-down Fe 3d orbitals (see Fig. S3(a)), resulting in a net magnetic moment in Fe_2SSeX_2. The effect of X atoms is to provide electrons to the S and Se atoms, analogous to the metal atoms decorated into the FeSe system, such as Li, K and Tl.[24–26,49] The two Fe atoms turn into Fe^+ ions with the valence electronic configuration $3d^74s^0$ after offering electrons to the S and Se atoms, as verified by related investigations.[50] Notably, the electrons of Fe^+ 4s move to the Fe^+ 3d orbitals on account of orbital hybridization, which can be found in many 2D materials.[51,52] From Fig. 2(c), the seven electrons of the Fe 3d orbitals are distributed in different orbitals ($d_{x^2-y^2}$, d_{xz}, d_{yz}, d_{xy} and d_{z^2}). We can understand the Fe d-orbital splitting sequence by the crystal-field theory of a tetragonal lattice, where the energy order is $d_{x^2-y^2} > d_{xy} > d_{xz}/d_{yz} > d_{z^2}$.

Compared with the Fe d_{xy} orbital, the energies of Fe d_{xz}/d_{yz} orbitals are higher because the S^{2-} and Se^{2-} ions have risen in the *xy* plane. The spin-up and spin-down states are split after introducing the exchange interaction, which generates half-occupied Fe $d_{x^2-y^2}$ and d_{xz}/d_{yz} orbitals (see Fig. 2(c)). So, the net magnetic moment per Fe atom is 3 μ_B.

In accordance with the Mermin–Wagner theorem[53], long-range magnetic ordering of 2D isotropic materials is usually prevented at nonzero temperatures. Therefore, in order to maintain the long-range FM ground state, magnetic anisotropy is vital for 2D systems. The magnetocrystalline anisotropy energy (MAE) can be employed to determine the magnetization orientation, which is defined as the total energy difference $E_{MAE} = E_{IP} - E_{OOP}$ between in-plane (IP) and OOP magnetization. A positive or negative MAE represents that the easy magnetic axis is along the OOP or IP direction, respectively. For Fe_2SSeX_2, the total energy (the energy along the IP magnetization is set as zero) versus angle (θ) between the magnetization orientation within the *xz* plane and the *z* axis is shown in Figs. 2(f)–2(h), and can be represented by[54]

$$E(\theta) = E_0 + K_1 \cos^2\theta + K_2 \cos^4\theta. \quad (2)$$

Here E_0 is the energy with the magnetization orientation along the easy magnetic axis; it is set as zero. K_1 and K_2 are system-related anisotropy constants and are summarized in Table 1. As displayed in Figs. 2(f)–2(h), we can clearly see that the MAEs of Fe_2SSeX_2 are closely related to the magnetization orientation of the *xz* plane and easy magnetic axis orientation along the IP direction. When the magnetization is perpendicular to the *xy* plane, the MAEs of Fe_2SSeGa_2, Fe_2SSeIn_2 and Fe_2SSeTl_2 are −177 μeV, −50 μeV and −4731 μeV, respectively; these can resist thermal fluctuation and hence are suitable for practical spintronic nanodevices. Analogous to the 2D materials CeI_2,[55] VSi_2N_4[56] and $VCSiN_4$,[57] Fe_2SSeX_2 have one easy magnetization plane. It is worth noting that no energetic barrier exists for rotation of the magnetic axis in the *xy* plane, and thus these materials are regarded as 2D *XY* magnets.

To assess the magnetic features of 2D FM materials, another significant factor is the Curie temperature or universal magnetic transition temperature. For one 2D *XY* square system, the Berezinsky–Kosterlitz–Thouless transition[58] can appear at a critical temperature (T), which is calculated by $T = 0.89J/k_B$, where k_B is the Boltzmann constant and J is the nearest-neighbor exchange parameter. J is obtained from the energy difference between the FM and AFM states (see Table 1) using a $2 \times 2 \times 1$ supercell, where $J = (E_{AFM} - E_{FM})/(32S^2)$. With $S = 1$, as listed in Table 1, T values for Fe_2SSeGa_2, Fe_2SSeIn_2 and Fe_2SSeTl_2 are predicted to be 755 K, 616 K and 506 K, respectively, which are higher than room temperature. All in all, due to the sizeable MAE and high T, Fe_2SSeX_2 compounds are considered to be prospective candidates for efficient spintronic devices.

The excellent T values are connected to the particular parent FeSe structure, which induces powerful super-exchange and direct-exchange interactions in Fe_2SSeX_2. As plotted in Fig. 2(d), the distances of the nearest-neighbor Fe–Fe atoms for Fe_2SSeGa_2, Fe_2SSeIn_2 and Fe_2SSeTl_2 are 2.71 Å, 2.73 Å and 2.79 Å, respectively, which are beneficial for large overlap of the Fe 3d orbitals. Generally, when the Fe 3d orbitals are almost completely occupied, the nearest-neighbor direct-exchange interactions (see Fig. 2(d)) are inclined to the FM coupling[54] because the electrons can be permitted to jump between the empty and filled orbitals with the same spin channel. The related physical mechanisms are shown in Fig. 2(e). Furthermore, in accordance with the Goodenough–Kanamori–Anderson super-exchange theory,[59–61] the super-exchange interactions between the next-nearest-neighbor Fe atoms by means of the S 3p and Se 4p orbitals (namely, Fe–S–Fe and Fe–Se–Fe) are FM coupling interactions (see Fig. 2(d)). The bond angles (α) of Fe–S–Fe and Fe–Se–Fe for Fe_2SSeGa_2, Fe_2SSeIn_2 and Fe_2SSeTl_2 are summarized in Table 1 and are close to 90°. Both super-exchange and direct-exchange with FM interactions cause Fe_2SSeX_2 to possess a high T value.

The electronic band structures of Fe_2SSeX_2 without and with SOC are displayed in Fig. 3. When SOC is excluded, the spin-down bands form one gapless Dirac semimetal (see Figs. 3(a)–3(c)). The spin-down bands link the conduction and valence bands, and the spin-up bands of Fe_2SSeGa_2, Fe_2SSeIn_2 and Fe_2SSeTl_2 have large gaps of 1.03 eV, 1.03 eV and 1.07 eV, respectively. In particular, the $d_{x^2-y^2}$ and d_{xy} orbitals of Fe atoms primarily contribute to the two spin-down channels near the Fermi level, where the M_x and M_y mirrors protect the Dirac cones along Γ–X and Γ–Y, respectively. Moreover, Fe_2SSeSX_2 are regarded as Weyl semimetals since the crossed bands in the Fermi level are 100% spin polarized,[10–12] analogous to the notion of half-metals.[62] The calculated Fermi velocities (υ_f) are listed in Table 1; these are comparable to the value for graphene (5.3×10^5 m·s^{-1}).[63] Completely spinpolarized Weyl semimetals with fine Fermi velocity can be applied as electrode devices and FM materials for manufacturing magnetic tunnel junctions[64] and spin field-effect transistors.[62] When OOP ferromagnetism is considered, the M_x and M_y mirrors are broken and the Weyl points disappear. Band gaps (E_g) of 174 meV, 199 meV and 112 meV are observed for Fe_2SSeGa_2, Fe_2SSeIn_2 and Fe_2SSeTl_2, respectively, as shown in Figs. 3(d)–3(f), implying that nontrivial topology may exist. When magnetization of the Fe atoms is reversed, the spin can be flipped (see Figs. 3(g)–3(i)). Notably, the large E_g can be ascribed to the boosted effective SOC strength of Fe 3d orbitals via bonding with the decorated heavy elements.[49]

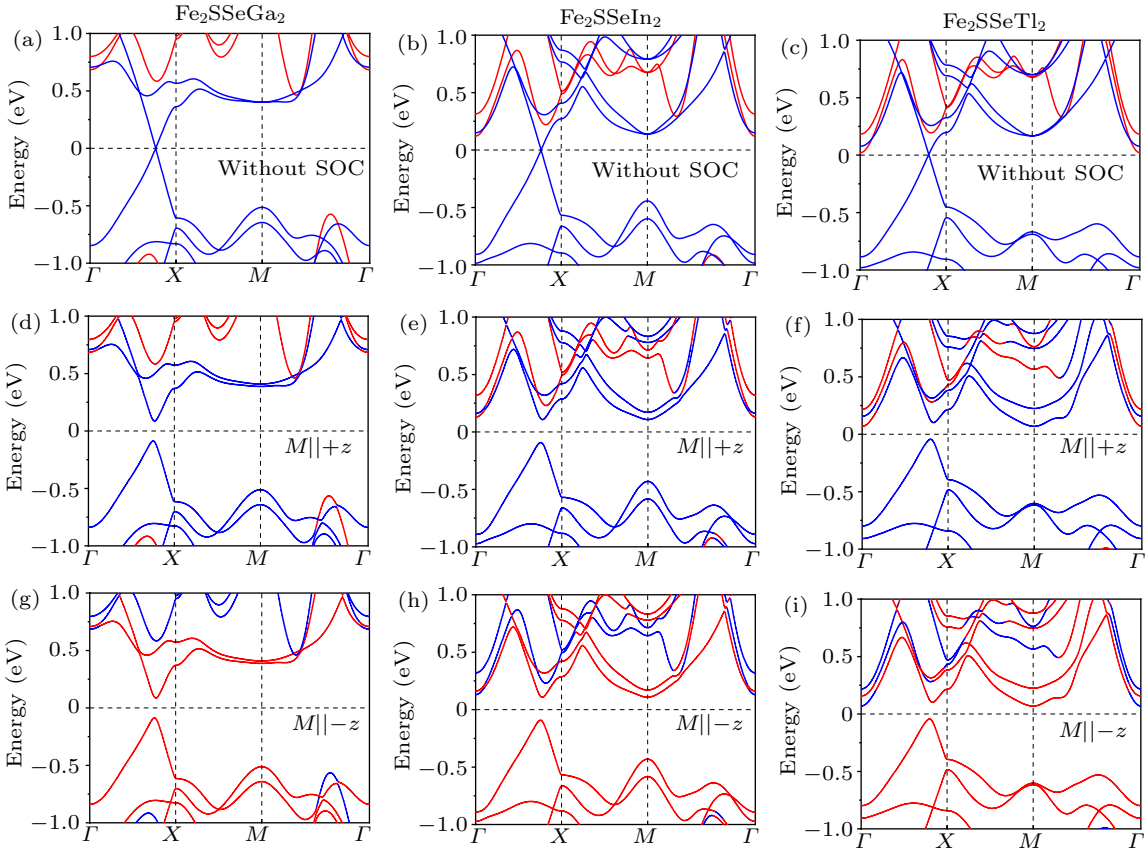


Fig. 3. (a)–(c) Band structures of Fe_2SSeGa_2, Fe_2SSeIn_2 and Fe_2SSeTl_2 without SOC, respectively. The band structures with SOC for the magnetization of Fe along the (d)–(f) $+z$ and (g)–(i) $-z$ directions. The blue and red lines denote spin-down and spin-up states, respectively.

For a material with certain magnetic order, when time-reversal symmetry is broken nontrivial topological properties can be proved by a nonzero Chern number (C), which is calculated by the following equation:

$$C = \frac{1}{2\pi}\int_{\mathrm{BZ}} \mathrm{d}^2k\Omega_z(k). \tag{3}$$

Here $\Omega_z(k)$ is the Berry curvature along the z direction, which is given by the Kudo formula[65] as

$$\Omega_z(k) = -\sum_n \sum_{n\neq n'} f_n \frac{2\,\mathrm{Im}\langle\psi_{nk}|\upsilon_x|\psi_{n'k}\rangle\langle\psi_{n'k}|\upsilon_y|\psi_{nk}\rangle}{(E_n - E_{n'})^2}, \tag{4}$$

where f_n is the Fermi–Dirac distribution function, $\upsilon_x(\upsilon_y)$ is the velocity operator and $\langle\psi_{nk}|$ is the Bloch wave function associated with the eigenvalue E_n. The distribution of $\Omega_z(k)$ in the 2D Brillouin zone for Fe_2SSeGa_2, Fe_2SSeIn_2 and Fe_2SSeTl_2 is plotted in Figs. 4(a), S4(a) and S5(a), respectively. Each gapped Dirac cone can contribute to the topological charge of 0.5, leading to $C = 2$ for the Janus monolayers Fe_2SSeX_2. As a marker of QAH systems, two chiral gapless edge states link the conduction and valence bands (see Figs. 4(c), S4(c) and S5(c)), which agrees with the consequences of $C = 2$. Since the Dirac cones are provided by spin-down channels, the edge states are also spin-down. When flipping the magnetization of Fe atoms, the edge states can be simultaneously changed (see Figs. 4(d), S4(d) and Fig. S5(d)), and are dominated by spin-up channels. In addition, as shown in Figs. 4(b), S4(b) and S5(b), $C = -2$ can be calculated. These discussions demonstrate that the edge states are 100% spin polarized, revealing that Fe_2SSeX_2 compounds possess the fascinating behavior of chiral spin–edge state locking. Therefore, multifunctional quantum devices may be fabricated from Fe_2SSeX_2.

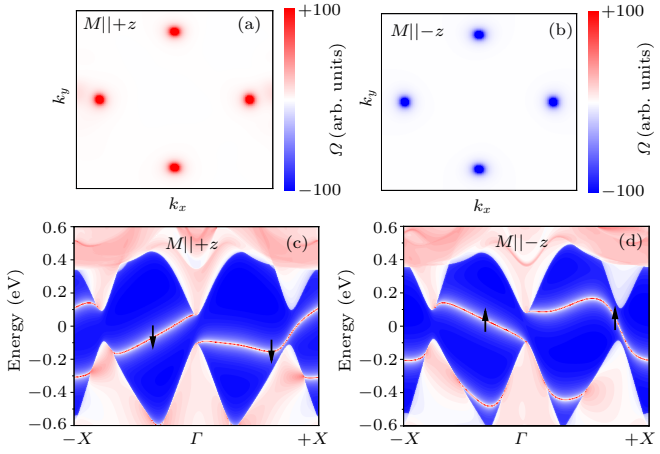


Fig. 4. (a), (b) Berry curvatures and (c), (d) edge states for Fe_2SSeGa_2 with the magnetization of Fe along the $+z$ and $-z$ directions.

Because the magnetization orientations of systems can be regulated under an external magnetic field,[66,67] we hope

that the phase transitions between QAH and Weyl semimetal states can be realized in Fe_2SSeGa_2. The band structures along different magnetization directions adjusted from the $+z$ axis ($\theta = 0^\circ$) to the $-z$ axis ($\theta = 180^\circ$) for Fe_2SSeGa_2 are plotted in Fig. S6. The significant traits are that the nontrivial band gaps are respectable (greater than the thermal energies at room temperature). The effective SOC strength of d orbitals is improved due to bonding with heavy atoms, and the SOC effects are obviously increased in the vicinity of the band crossing points, which generate sizable nontrivial band gaps. On account of the powerful interactions between topology and magnetism, the nontrivial band gaps can be tuned by an external magnetic field. When the magnetization orientation is varied from $+z$ to $+x$ then to $-z$, the gap decreases to zero and then increases (see Figs. 5(a)–5(c)), similar to previous reports.[10] For Fe_2SSeX_2, when $\theta = 90^\circ$ Weyl semimetal states can be realized. Furthermore, we can observe the occurrence of topological phase transitions from $C = 2$ to $C = -2$. Besides, nontrivial topological properties with different C may be gained for general IP magnetization with broken mirror symmetry.[68]

It has been discovered that strain is an effective means to regulating the electronic and magnetic properties of 2D systems.[57] Biaxial strain (η) is defined as $\eta = (m - m_0)/m_0$, where m (m_0) is the lattice constant with (without) strain. As listed in Tables S1–S3, Fe_2SSeX_2 always prefer FM coupling with $-5\% \leq \eta \leq +5\%$. The effect strain on the electronic properties was explored. For OOP magnetization, according to Fig. S7, Fe_2SSeGa_2 always manifests semiconducting features with sizable band gaps (136–181 meV) (see Fig. 5(d)) in the investigated strain range. However, the band gaps of the Fe_2SSeIn_2 and Fe_2SSeTl_2 are 89–199 meV (see Fig. 5(e)) and 64–145 meV (see Fig. 5(f)). In order to substantiate these nontrivial band gaps, we take Fe_2SSeGa_2 as an example and calculate the strained edge states. As plotted in Fig. S8, they all have two chiral nontrivial edge states connecting the valence and conduction bands for $-5\% \leq \eta \leq +5\%$, demonstrating that the QAH features of Fe_2SSeX_2 are robust against strain. The MAEs as a function of strain are shown in Figs. 5(g)–5(i). Significantly, for a compressive strain of $-5\% \leq \eta \leq -1\%$, the easy magnetic axis directions of Fe_2SSeGa_2 and Fe_2SSeIn_2 are regulated from IP to OOP, indicating that nontrivial band topology can spontaneously occur in Fe_2SSeGa_2 and Fe_2SSeIn_2.

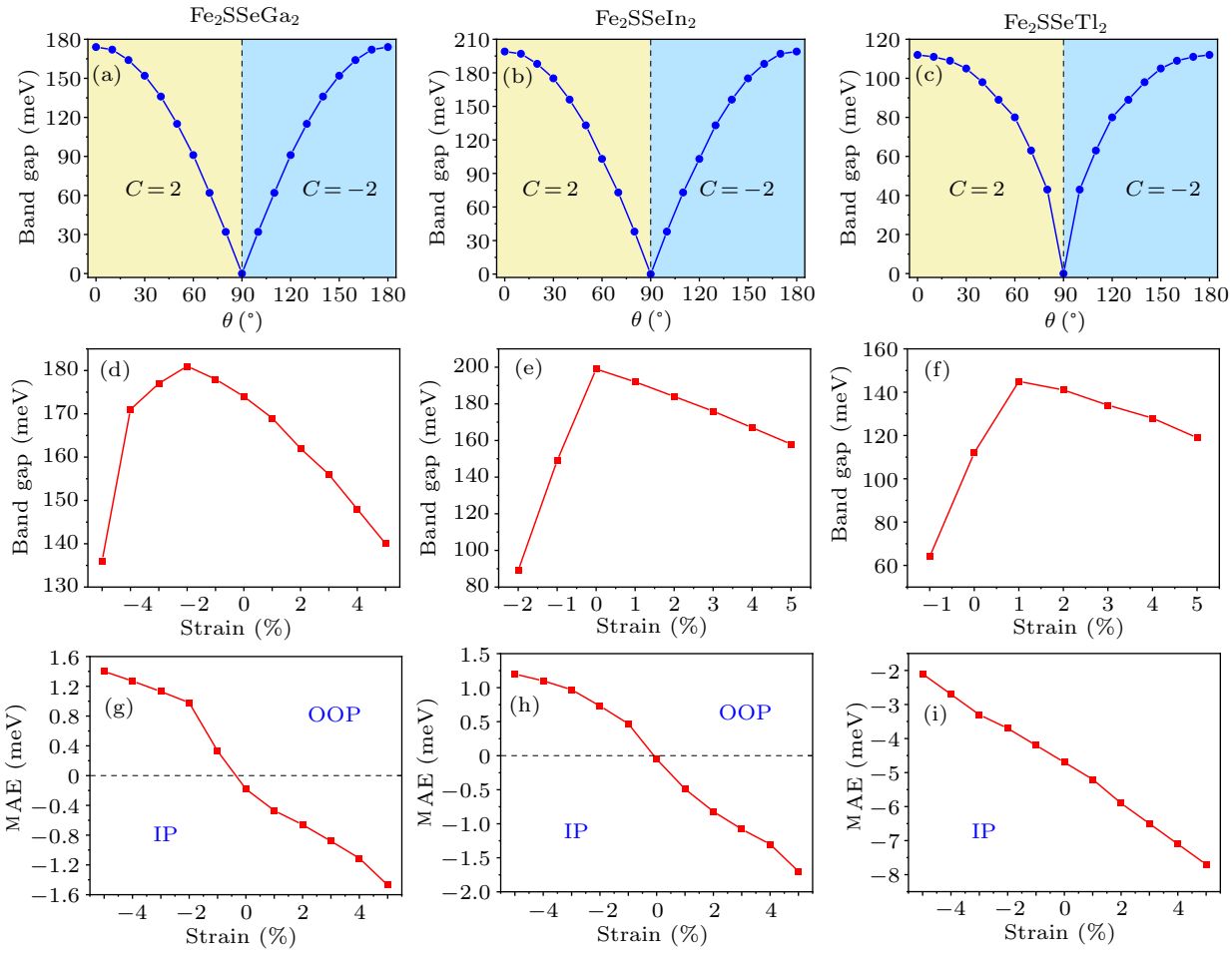


Fig. 5. (a)–(c) The band gap and Chern number (C) as a function of polar angle θ. Here, $\theta = 0^\circ$, 90° and 180°represent $+z$, $+x$ and $-z$ orientations, respectively. (d)–(f) The band gap as a function of strain. (g)–(i) The magnetocrystalline anisotropy energy (MAE) as a function of strain. IP, in-plane magnetization; OOP, out-of-plane magnetization.

4. Conclusion

In conclusion, we have performed comprehensive research into the structural, electronic, magnetic and topological properties of Fe_2SSeX_2 by first-principles calculations. These compounds are forecast to be fascinating QAH insulators. The nontrivial topological properties were verified by the Berry curvatures, two chiral edge states and nonzero Chern-number $C = 2$. The interesting behavior of chiral spin-edge state locking can be found, because when the magnetization is flipped the Dirac cones are determined by spin-up channels and $C = -2$ can be achieved. We observed that the QAH properties are robust against strain. Nontrivial topological properties can spontaneously appear when strain is applied. Our work provides ideal candidate materials to realize high-performance quantum topological devices and new research ideas for the combination of superconductivity and topology.

Acknowledgements

Project supported by the National Natural Science Foundation of China (Grant Nos. 52173283 and 62071200), Taishan Scholar Program of Shandong Province (Grant No. ts20190939), and Independent Cultivation Program of Innovation Team of Jinan City (Grant No. 2021GXRC043).

References

[1] Haldane F D M 2017 *Rev. Mod. Phys.* **89** 040502
[2] Hasan M Z and Kane C L 2010 *Rev. Mod. Phys.* **82** 3045
[3] Qi X L and Zhang S C 2011 *Rev. Mod. Phys.* **83** 1057
[4] Haldane F D M 1988 *Phys. Rev. Lett.* **61** 2015
[5] Li T, Jiang S, Shen B, Zhang Y, Li L, Tao Z, Devakul T, Watanabe K, Taniguchi T, Fu L, Shan J and Mak K F 2021 *Nature* **600** 641
[6] Deng Y, Yu Y, Shi M Z, Guo Z, Xu Z, Wang J, Chen X H and Zhang Y 2020 *Science* **367** 895
[7] Serlin M, Tschirhart C L, Polshyn H, Zhang Y, Zhu J, Watanabe K, Taniguchi T, Balents L and Young A F 2020 *Science* **367** 900
[8] Chiu C K, Teo J C Y, Schnyder A P and Ryu S 2016 *Rev. Mod. Phys.* **88** 035005
[9] Armitage N P, Mele E J and Vishwanath A 2018 *Rev. Mod. Phys.* **90** 015001
[10] You J Y, Chen C, Zhang Z, Sheng X L, Yang S A and Su G 2019 *Phys. Rev. B* **100** 064408
[11] Li G G, Xie R R, Ding L J, Ji W X, Li S S, Zhang C W, Li P and Wang P J 2021 *Phys. Chem. Chem. Phys.* **23** 12068
[12] Jin L, Wang L, Zhang X, Liu Y, Dai X, Gao H and Liu G 2021 *Nanoscale* **13** 5901
[13] Zhang S J, Zhang C W, Zhang S F, Ji W X, Li P, Wang P J, Li S S and Yan S S 2017 *Phys. Rev. B* **96** 205433
[14] Li S S, Ji W X, Hu S J, Zhang C W and Yan S S 2017 *ACS Appl. Mater. Interfaces* **9** 41443
[15] Jia K, Dong X J, Li S S, Ji W X and Zhang C W 2023 *Nanoscale* **15** 8395
[16] Wu B, Song Y L, Ji W X, Wang P J, Zhang S F and Zhang C W 2023 *Phys. Rev. B* **107** 214419
[17] Han Y T, Ji W X, Wang P J, Li P and Zhang C W 2023 *Nanoscale* **15** 6830
[18] Jia K, Dong X J, Li S S, Ji W X and Zhang C W 2023 *ACS Appl. Nano Mater.* **6** 14003
[19] Sun H, Li S S, Ji W X and Zhang C W 2022 *Phys. Rev. B* **105** 195112
[20] Jia K, Dong X J, Li S S, Ji W X and Zhang C W 2024 *Nanoscale* **16** 8639
[21] Song C L, Wang Y L, Jiang Y P, Li Z, Wang L, He K, Chen X, Ma X C and Xue Q K 2011 *Phys. Rev. B* **84** 020503
[22] Fang M H, Wang H D, Dong C H, Li Z J, Feng C M, Chen J and Yuan H Q 2011 *Europhys. Lett.* **94** 27009
[23] Burrard-Lucas M, Free D G, Sedlmaier S J, Wright J D, Cassidy S J, Hara Y, Corkett A J, Lancaster T, Baker P J, Blundell S J and Clarke S J 2013 *Nat. Mater.* **12** 15
[24] He S, He J, Zhang W, *et al.* 2013 *Nat. Mater.* **12** 605
[25] Tan S, Zhang Y, Xia M, Ye Z, Chen F, Xie X, Peng R, Xu D, Fan Q, Xu H, Jiang J, Zhang T, Lai X, Xiang T, Hu J, Xie B and Feng D 2013 *Nat. Mater.* **12** 634
[26] Ge J F, Liu Z L, Liu C, Gao C L, Qian D, Xue Q K, Liu Y and Jia J F 2015 *Nat. Mater.* **14** 285
[27] He K, Wang Y and Xue Q K 2018 *Annu. Rev. Condens. Matter Phys.* **9** 329
[28] Ren Y, Qiao Z and Niu Q 2016 *Rep. Prog. Phys.* **79** 066501
[29] König M, Wiedmann S, Brüne C, Roth A, Buhmann H, Molenkamp L W, Qi X L and Zhang S C 2007 *Science* **318** 766
[30] Kane C L and Mele E J 2005 *Phys. Rev. Lett.* **95** 226801
[31] Chen P, Pai W W, Chan Y H, Sun W L, Xu C Z, Lin D S, Chou M Y, Fedorov A V and Chiang T C 2018 *Nat. Commun.* **9** 2003
[32] Ge J, Liu Y, Li J, Li H, Luo T, Wu Y, Xu Y and Wang J 2020 *Natl. Sci. Rev.* **7** 1280
[33] Miert G V, Smith C M and Juricic V 2014 *Phys. Rev. B* **90** 081406
[34] Cai T, Li X, Wang F, Ju S, Feng J and Gong C D 2015 *Nano Lett.* **15** 6434
[35] Song Y J, Ahn K H, Pickett W E and Lee K W 2016 *Phys. Rev. B* **94** 125134
[36] Kong X, Li L, Leenaerts O, Wang W, Liu X J and Peeters F M 2018 *Nanoscale* **10** 8153
[37] Blochl P E 1994 *Phys. Rev. B* **50** 17953
[38] Kresse G and Hafner J 1994 *Phys. Rev. B* **49** 14251
[39] Kresse G and Furthmuller J 1996 *Phys. Rev. B* **54** 11169
[40] Perdew J P, Burke K and Ernzerhof M 1996 *Phys. Rev. Lett.* **77** 3865
[41] Dudarev S L, Botton G A, Savrasov S Y, Humphreys C J and Sutton A P 1998 *Phys. Rev. B* **57** 1505
[42] Liu G, Chen T, Zhou G, Xu Z and Xiao X 2023 *ACS Sens.* **8** 1440
[43] Wu X, Vanderbilt D and Hamann D R 2005 *Phys. Rev. B* **72** 035105
[44] Togo A, Oba F and Tanaka I 2008 *Phys. Rev. B* **78** 134106
[45] Mostofi A A, Yates J R, Lee Y S, Souza I, Vanderbilt D and Marzari N 2008 *Comput. Phys. Commun.* **178** 685
[46] Wang X, Yates J R, Souza I and Vanderbilt D 2006 *Phys. Rev. B* **74** 195118
[47] Wu Q, Zhang S, Song H F, Troyer M and Soluyanov A A 2018 *Comput. Phys. Commun.* **224** 405
[48] Lu A Y, Zhu H, Xiao J, *et al.* 2017 *Nat. Nanotechnol.* **12** 744
[49] Li Y, Li J H, Li Y, Ye M, Zheng F W, Zhang Z T, Fu J H, Duan W H and Xu Y 2020 *Phys. Rev. Lett.* **125** 086401
[50] Yu M and Trinkle D R 2011 *J. Chem. Phys.* **134** 064111
[51] Cao C, Wu M, Jiang J and Cheng H P 2010 *Phys. Rev. B* **81** 205424
[52] Wehling T O, Lichtenstein A I and Katsnelson M I 2011 *Phys. Rev. B* **84** 235110
[53] Mermin N D and Wagner H 1966 *Phys. Rev. Lett.* **17** 1133
[54] Coey J M D 2010 *Magnetism and Magnetic Materials* (Cambridge: Cambridge University Press)
[55] Sheng K, Chen Q, Yuan H K and Wang Z Y 2022 *Phys. Rev. B* **105** 075304
[56] Cui Q R, Zhu Y M, Liang J H, Cui P and Yang H X 2021 *Phys. Rev. B* **103** 085421
[57] Jia K, Dong X J, Li S S, Ji W X and Zhang C W 2023 *J. Mater. Chem. C* **11** 10359
[58] Fernández J F, Ferreira M F and Stankiewicz J 1986 *Phys. Rev. B* **34** 292
[59] Goodenough J B 1955 *Phys. Rev.* **100** 564
[60] Anderson P W 1959 *Phys. Rev.* **115** 2
[61] Kanamori J 1960 *J. Appl. Phys.* **31** S14
[62] utic I, Fabian J and Das Sarma S 2004 *Rev. Mod. Phys.* **76** 323
[63] Wang Y L and Ding Y 2013 *Solid State Commun.* **155** 6
[64] Jin Y, Yan M, Dedkov Y and Voloshina E 2022 *J. Mater. Chem. C* **10** 3812
[65] Thouless D J, Kohmoto M, Nightingale M P and den Nijs M 1982 *Phys. Rev. Lett.* **49** 405
[66] Nie S, Sun Y, Prinz F B, Wang Z, Weng H, Fang Z and Dai X 2020 *Phys. Rev. Lett.* **124** 076403
[67] Wu M 2017 *2D Mater.* **4** 021014
[68] Liu X, Hsu H C and Liu C X 2013 *Phys. Rev. Lett.* **111** 086802